28. Field, L. & Engelhardt, P. R. Organic disulfides and related substances. XXX. Preparations and reactions of mercaptoterephthalic acids and derivatives. *J. Org. Chem.* **35,** 3647–3654 (1970).
29. Fang, X., Mark, G. & von Sonntag, C. OH radical formation by ultrasound in aqueous solutions. Part 1: the chemistry underlying the terephthalate dosimeter. *Ultrason. Sonochem.* **3,** 57–63 (1996).
30. Damiani, P. & Burini, G. Fluorometric determination of nitrite. *Talanta* **33,** 649–652 (1986).
31. Matula, T. J. *et al.* The acoustic emission from single-bubble sonoluminescence. *J. Acoust. Soc. Am.* **103,** 1377–1382 (1998).

Acknowledgements

We thank W.B. McNamara III for discussions. This work was supported by the US Defense Advanced Research Project Agency and in part by the National Science Foundation. We thank the UIUC Laboratory for Fluorescence Dynamics for use of their facilities.

Competing interests statement

The authors declare that they have no competing financial interests.

Correspondence and requests for materials should be addressed to K.S.S. (e-mail: ksuslick@uiuc.edu).

Equilibrium lithium transport between nanocrystalline phases in intercalated TiO_2 anatase

M. Wagemaker*, A. P. M. Kentgens† & F. M. Mulder*

* *Interfaculty Reactor Institute, Delft University of Technology, Mekelweg 15, 2629 JB Delft, The Netherlands*
† *NSR Center for Molecular Design, Synthesis and Structure, Department of Physical Chemistry/Solid-state NMR, University of Nijmegen, Toernooiveld 1, 6525 ED Nijmegen, The Netherlands*

Microcrystalline TiO_2 with an anatase crystal structure is used as an anode material for lithium rechargeable batteries[1,2], and also as a material for electrochromic[3–6] and solar-cell devices[7,8]. When intercalated with lithium, as required for battery applications, TiO_2 anatase undergoes spontaneous phase separation into lithium-poor ($Li_{0.01}TiO_2$) and lithium-rich ($Li_{0.6}TiO_2$) domains on a scale of several tens of nanometres[9]. During discharge, batteries need to maintain a constant electrical potential between their electrodes over a range of lithium concentrations. The two-phase equilibrium system in the electrodes provides such a plateau in potential, as only the relative phase fractions vary on charging (or discharging) of the lithium. Just as the equilibrium between a liquid and a vapour is maintained by a continuous exchange of particles between the two phases, a similar exchange is required to maintain equilibrium in the solid state. But the time and length scales over which this exchange takes place are unclear. Here we report the direct observation by solid-state nuclear magnetic resonance of the continuous lithium-ion exchange between the intermixed crystallographic phases of lithium-intercalated TiO_2. We find that, at room temperature, the continuous flux of lithium ions across the phase boundaries is as high as $1.2 \times 10^{20}\ s^{-1}\ m^{-2}$.

We used ^{7}Li magic-angle-spinning (MAS) solid-state NMR, because this microscopic probe gives information on structure and dynamics[10,11]. The anatase starting material had a particle size of ~10 μm (nitrogen BET specific surface area $<0.5\ m^2\ g^{-1}$). In Fig. 1, the central part of the ^{7}Li MAS NMR spectrum of a lithium-intercalated sample, $Li_{0.12}TiO_2$, is shown. In this sample, two phases coexist[9]: the lithium-poor phase $Li_{0.01}TiO_2$ with the anatase structure (space group $I41/amd$), and the lithium-rich phase indicated by lithium titanate ($Li_{0.6}TiO_2$; space group $Imma$). The Li in anatase gives a sharp line in addition to the broad Li in titanate signal.

The exchange of Li between the two phases is established by performing two-dimensional exchange measurements[12]. This technique effectively measures the spectrum of the ^{7}Li atoms at $t = 0$ s, then waits a 'mixing time' t_{mix}, and subsequently measures the spectrum of the same ^{7}Li atoms again at $t = t_{mix}$. The results of such measurements are shown in Fig. 2. The signal occurring on the diagonal in the plots represents ^{7}Li atoms that have the same spectrum before and after t_{mix}—that is, ^{7}Li that remained in the same crystallographic phase. The spectral intensity produced by ^{7}Li that is located in anatase at $t = 0$ and in titanate at $t = t_{mix}$ (or *vice versa*) is at the corresponding off-diagonal positions. The ridges in Fig. 2b are off-diagonal signals of this type; they are strong because of the large amount of Li that has exchanged between the two phases within the diffusion time of $t_{mix} = 50$ ms.

In Fig. 2a $t_{mix} = 50$ μs, which means virtually no diffusion time, and thus no exchange. Because about 40% of the intensity in the sharp peak in Fig. 2a is transferred to intensity in the ridges in Fig. 2b, about 40% of the initial amount of ^{7}Li in anatase has exchanged with ^{7}Li in the titanate phase after $t_{mix} = 50$ ms, as can be seen when comparing Fig. 2a and b. In Fig. 2c, a measurement is shown at 148 K using a t_{mix} of 50 ms. At this temperature the Li motion between anatase and titanate is frozen. But there still appears to be diffusion within the titanate phase; this will be due to the low activation energy for hopping between sites within this phase[9]. The measurement is shown here to prove that the cross-signal intensities in Fig. 2b cannot arise from spin diffusion due to the presence of dipolar couplings (these are suppressed by MAS).

Faster one-dimensional experiments were performed to quantify the exchange in terms of the magnetization of Li in anatase as a function of t_{mix} and temperature T. The technique is described in Fig. 3 legend. The experimental results in Fig. 3 are given as a function of t_{mix}, and for several temperatures. The data are analysed using the solution of Fick's law of diffusion, $\partial m(\mathbf{r},t)/\partial t = \nabla\cdot\{D(\mathbf{r})m(\mathbf{r},t)\}$, where $m(\mathbf{r},t)$ is the magnetization of Li at position $\mathbf{r}$ and t, and D is the Li diffusivity. Best results were obtained with

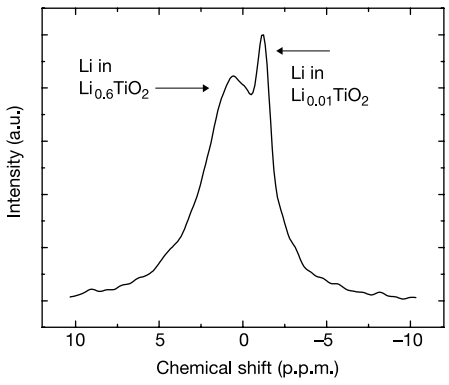

Figure 1 Central part of the ^{7}Li magic-angle-spinning NMR spectrum of $Li_{0.12}TiO_2$ at 100 °C, showing the resonances of Li in the two coexisting phases. A spinning speed of 20,000 ± 3 Hz and a radio-frequency field strength corresponding to a ^{7}Li spin nutation frequency of 192 kHz was used on a Chemagnetics 600 spectrometer. Two phases are coexisting in thermal equilibrium: a Li-poor anatase phase with a composition of $Li_{0.01}TiO_2$ (narrow peak) and a Li-rich titanate phase with composition $Li_{0.6}TiO_2$ (this peak is homogeneously broadened, with the transverse relaxation time T_2 giving its linewidth, indicating that the ^{7}Li in this phase are all experiencing similar environments).

isotropic diffusion in three dimensions, which agrees with the data of ref. 13, and the single-crystal data of ref. 14. Using the mathematics of the models for spin diffusion[15,16], and assuming (for simplicity) the overall diffusivity to be isotropic and spatially independent, the rate of demagnetization of a cube of phase A (anatase), initial magnetization m_{A0}, and dimension d_A, owing to diffusion of magnetized Li towards the surrounding unmagnetized phase B (titanate), can be derived as:

$$m_A(t_{mix}) = \frac{m_{A,0}}{(c_A + c_B)^3}\left\{2d_A c_A + c_B\sqrt{4Dt_{mix}}\left[\mathrm{ierfc}\left(\frac{d_A}{\sqrt{4Dt_{mix}}}\right) + \mathrm{ierfc}\left(\frac{-d_A}{\sqrt{4Dt_{mix}}}\right) - \frac{2}{\sqrt{\pi}}\right]\right\}^3$$

Here $\mathrm{ierfc}(x) = (1/\sqrt{\pi})\exp(-x^2) - x(1 - \mathrm{erf}(x))$, and $c_A^3 = 0.01$ and $c_B^3 = 0.60$ represent the Li concentrations in anatase and titanate, respectively, which were determined previously[9]. The dimension of the anatase domains was determined[9] from the width of X-ray diffraction peaks to be about 60 ± 15 nm. The only remaining fitting parameter in the model is the diffusion rate, D, for the diffusion of Li in the anatase and titanate system.

The fits are shown in the top panel of Fig. 3. The bottom part of Fig. 3 gives an Arrhenius plot of the temperature dependence of D. An activation energy of 0.45 ± 0.06 eV can be deduced for the overall cross-boundary diffusion, which is close to the value found from macroscopic Li diffusion data[13]. Recent first-principles calculations yielded a similar value for the activation energy for the growth of the Li-rich phase on Li intercalation[17].

The current density of Li flowing back and forth between the two phases can be determined from the timescale at which Li crosses the boundary, and from the surface areas of the ~60-nm-diameter spheres of anatase. At room temperature a value of $1.2 \times 10^{20}\,\mathrm{s^{-1}\,m^{-2}}$ is calculated. At 373 K the system is clearly highly dynamic on timescales much greater than 50 ms, and we suggest that the boundaries of the two phases will be non-stationary if not every Li diffusing to the other phase is replaced at exactly the same position. On such timescales, this would lead to diffusive

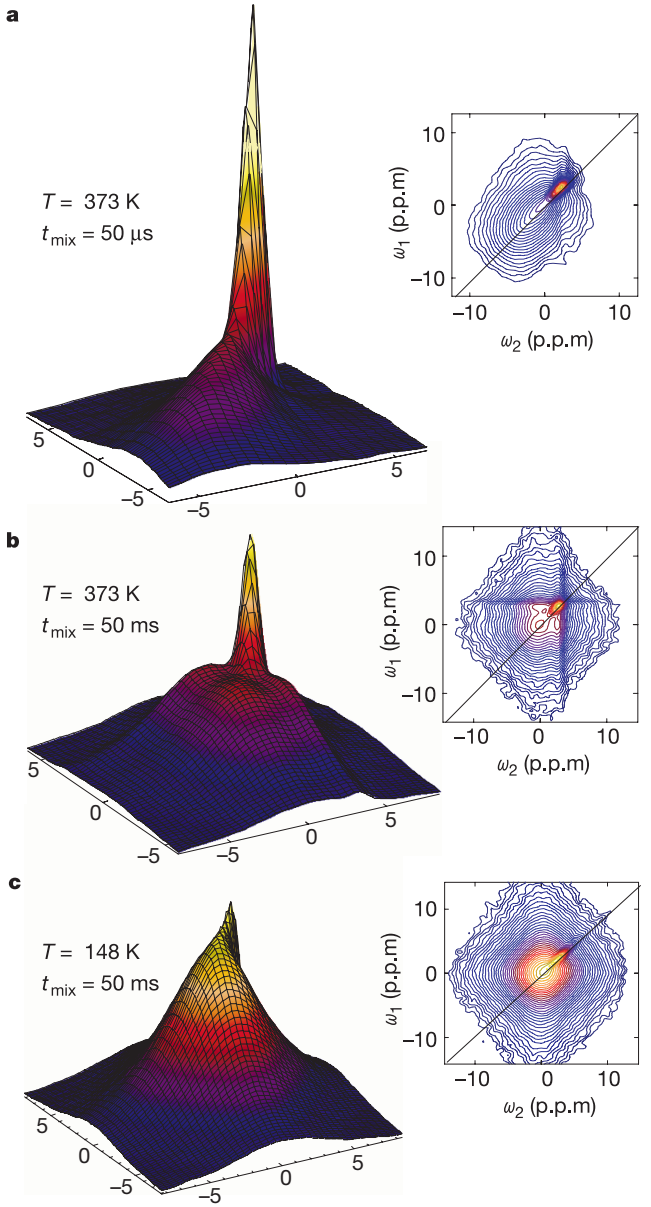

Figure 2 Exchange of Li between the two coexisting phases in $Li_{0.12}TiO_2$ measured with ^{7}Li two-dimensional exchange NMR. The contour plots (insets) are projections of the three-dimensional representations; ω_1 and ω_2 represent the chemical shift before and after t_{mix} respectively. **a**, At $T = 373$ K and $t_{mix} = 50\,\mu$s (see text) there are no cross-signal intensities visible, indicating that the diffusion time of 50 µs is still too short for cross-boundary lithium diffusion. **b**, At $T = 373$ K and $t_{mix} = 50$ ms, there are large ridges visible covering the widths of the Li in titanate signal at the position of the Li in anatase signal. These cross-signal intensities are a direct measure of cross-boundary Li diffusion. **c**, At $T = 148$ K and $t_{mix} = 50$ ms, the cross-boundary lithium diffusion is absent owing to freezing of Li motion in the anatase phase. The rectangular off-diagonal shape of the Li in titanate peak shows that there is still diffusion within the titanate phase.

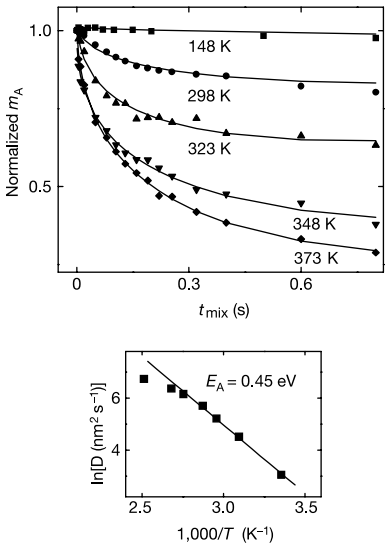

Figure 3 Quantifying the diffusion process. Top, time dependence of ^{7}Li magnetization in the anatase phase, indicating Li diffusion towards the titanate phase. The one-dimensional NMR pulse sequence $\pi/2$, τ, π, τ, $-\pi/2$, t_{mix}, $+\pi/2$, acquisition, was used, with the appropriate phase cycles for cancellation of direct magnetization that may occur after T_1 relaxation. (T_1 is the longitudinal relaxation time.) Using appropriate values of τ, the intensity of the narrow anatase line was conserved while that of the broad titanate line vanishes (T_2 filtering): that is, before t_{mix} starts, magnetization is only present in the anatase phase. Diffusion of lithium into the titanate phase during t_{mix} causes the normalized intensity $m_A(t_{mix})$ of the narrow anatase line to decrease strongly as a function of t_{mix}, while the broad titanate line becomes populated again. The lines represent fits using a Li diffusion model described in the text. Bottom, the temperature dependence of the diffusion parameter D. Using an Arrhenius behaviour, an activation energy E_A of 0.45 ± 0.06 eV is determined for the cross-boundary diffusion process.

motion of crystalline domains in an otherwise rigid solid-state system. □

Received 7 January; accepted 10 June 2002; doi:10.1038/nature00901.

1. Huang, S. Y., Kavan, L., Exnar, I. & Grätzel, M. J. Rocking chair lithium battery based on nanocrystalline TiO_2 (anatase). *J. Electrochem. Soc.* **142,** L142–L144 (1995).
2. Ohzuku, T., Kodama, T. & Hirai, T. Electrochemistry of anatase titanium dioxide in lithium non-aqueous cells. *J. Power Sources* **14,** 153–166 (1985).
3. Ohzuku, T. & Hirai, T. An electrochromic display based on titanium dioxide. *Electrochim. Acta* **27,** 1263–1266 (1982).
4. Ottaviani, M., Panero, S., Morzilli, S. & Scrosati, B. The electrochromic characteristics of titanium oxide thin film electrodes. *Solid State Ionics* **20,** 197–202 (1986).
5. Cantao, M. P., Cisneros, J. I. & Torresi, R. M. Electrochromic behaviour of sputtered titanium-oxide thin-films. *Thin Solid Films* **259,** 70–74 (1995).
6. Bechinger, C., Ferrere, S., Zaban, A., Sprague, J. & Gregg, B. A. Photoelectrochromic windows and displays. *Nature* **383,** 608–610 (1996).
7. O'Regan, B. & Grätzel, M. A low-cost, high-efficiency solar-cell based on dye-sensitised colloidal TiO_2 films. *Nature* **353,** 737–740 (1991).
8. Hagfeldt, A. & Grätzel, M. Light-induced redox reactions in nanocrystalline systems. *Chem. Rev.* **95,** 49–68 (1995).
9. Wagemaker, M., van de Krol, R., Kentgens, A. P. M., van Well, A. A. & Mulder, F. M. Two phase morphology limits lithium diffusion in TiO_2 (anatase): A Li-7 MAS NMR study. *J. Am. Chem. Soc.* **46,** 11454–11461 (2001).
10. Xu, Z. & Stebbins, J. F. Cation dynamics and diffusion in lithium orthosilicate — 2-dimensional Li-6 NMR. *Science* **270,** 1332–1334 (1995).
11. Verhoeven, V. W. J. *et al.* Lithium dynamics in $LiMn_2O_4$ probed directly by two-dimensional Li-7 NMR. *Phys. Rev. Lett.* **86,** 4314–4317 (2001).
12. Ernst, R. R., Bodenhausen, G. & Wokaun, A. *Principles of Nuclear Magnetic Resonance in One and Two Dimensions* (Clarendon, Oxford, 1994).
13. Lunell, S., Stashans, A., Ojamae, L., Lindstrom, H. & Hagfeldt, A. Li and Na diffusion in TiO_2 from quantum chemical theory versus electrochemical experiment. *J. Am. Chem. Soc.* **119,** 7374–7380 (1997).
14. Kavan, L., Grätzel, M., Gilbert, S. E., Klemenz, C. & Schell, H. J. Electrochemical and photoelectrochemical investigation of single-crystal anatase. *J. Am. Chem. Soc.* **118,** 6716–6723 (1996).
15. Claus, J., Schmidt-Rohr, K. & Spiess, H. W. Determination of domain sizes in heterogeneous polymers by solid-state NMR. *Acta Polym.* **44,** 1–17 (1993).
16. Schmidt-Rohr, K. & Spiess, H. W. *Multidimensional Solid-state NMR and Polymers* (Academic, London, 1994).
17. Koudriachova, M. V., Harrison, N. M. & de Leeuw, S. W. Effect of diffusion on lithium intercalation in titanium dioxide. *Phys. Rev. Lett.* **86,** 1275–1278 (2001).

Acknowledgements

This work is a contribution from the Delft Institute for Sustainable Energy (DISE).

Competing interests statement

The authors declare that they have no competing financial interests.

Correspondence and requests for materials should be addressed to F.M.M. (e-mail: mulder@iri.tudelft.nl).

Synthetic hosts by monomolecular imprinting inside dendrimers

Steven C. Zimmerman*†, Michael S. Wendland*, Neal A. Rakow*, Ilya Zharov† & Kenneth S. Suslick*†

** Department of Chemistry; † Beckman Institute for Advanced Science and Technology, University of Illinois at Urbana-Champaign, 600 S. Mathews Avenue, Urbana, Illinois 61801, USA*

Synthetic host systems capable of selectively binding guest molecules are of interest for applications ranging from separations and chemical or biological sensing to the development of biomedical materials. Such host systems can be efficiently prepared by 'imprinting' polymers or inorganic materials with template molecules, which, upon removal, leave behind spatially arranged functional groups that act as recognition sites[1–4]. However, molecularly imprinted polymers have limitations, including incomplete template removal, broad guest affinities and selectivities, and slow mass transfer[5–8]. An alternative strategy for moulding desired recognition sites uses combinatorial libraries of assemblies that are made of a relatively small number of molecules, interconverting in dynamic equilibrium; upon addition of a target molecule, the library equilibrium shifts towards the best hosts[9–11]. Here we describe the dynamic imprinting of dendritic macromolecules with porphyrin templates to yield synthetic host molecules containing one binding site each. The process is based on our general strategy to prepare cored dendrimers[12,13], and involves covalent attachment of dendrons to a porphyrin core, cross-linking of the end-groups of the dendrons, and removal of the porphyrin template by hydrolysis. In contrast to more traditional polymer imprinting, our approach ensures nearly homogeneous binding sites and quantitative template removal. Moreover, the hosts are soluble in common organic solvents and amenable to the incorporation of other functional groups, which should facilitate further development of this system for novel applications.

When developing our 'monomolecular imprinting' methodology, we selected dendrimers as macromolecular hosts because their molecular homogeneity and excellent solubility facilitate characterization[14]. The choice of a porphyrin as templating agent was motivated by the scarce availability of synthetic hosts for large molecule guests[15] and the fact that porphyrins are excellent probes of binding, owing to the sensitivity of their intense colour to the local environment[16]. Porphyrins have been integrated into molecularly imprinted polymers[17] and synthetic hosts[18], but have to our knowledge not been used as templates. Moreover, the chemistry of porphyrin-core dendrimers is well established, given their role as well-studied synthetic models of haem proteins and related proteins[19–22].

The basic strategy for synthesizing dendrimer hosts follows our earlier work on cored dendrimers[12,13]. The preparation of porphyrin-core dendrimer **1** is summarized in Fig. 1. The key structural features of this pre-cross-linked dendrimer are the tetrakis-meso(3,5-dihydroxyphenyl)-porphyrin (**3**)[19] unit at the core, and hydrolysable ester-bond links to eight third-generation Fréchet-type dendrons[23] (**2**)[12], which give a total of 64 homoallyl end-groups (see Supplementary Information). In addition to **1**, a small amount (~5%) of dendrimers containing six or seven dendrons was formed (see below).

Porphyrin-core dendrimer **1** was cross-linked[12] using 4 mol% (per alkene) of Grubbs' catalyst **4**[24] at 10^{-6} M in benzene to produce cross-linked dendrimer **5** in 88% yield. Size exclusion chromatography (SEC) established that cross-linking occurs largely (≥95%) intramolecularly. The ^{1}H NMR spectrum of **5** confirmed the formation of internal, disubstituted alkene groups and gave the average number of cross-links as approximately 29. The matrix-assisted laser desorption/ionization–time of flight (MALDI–TOF) mass spectrum of **5** provided conclusive evidence for extensive intramolecular cross-linking: it contained peaks corresponding to individual isomers from 28 to 32 out of 32 possible cross-links (mass/charge ratios (m/z) 10,369, 10,341, 10,313, 10,285, 10,257), with the tallest peak at m/z 10,285 (31 cross-links, see Supplementary Information). The ability of catalyst **4** to produce from **1** a compact structure with a median of 30 out of 32 possible cross-links may be due to the reversibility of the ring closing metathesis (RCM) reaction[24]. The precise details of the cross-linking process remain to be determined. But analogy with the quantitative RCM of polyolefins[25] suggests that it may be a dynamic process, thus ensuring that millions of kinetically favoured cross-link isomers may equilibrate into a small number of thermodynamically stable ones.

Treatment of the cross-linked dendrimer **5** with 2.5 M aqueous KOH solution in tetrahydrofuran (THF) quantitatively removed the porphyrin template (that is, **3**), forming **6** in a 43% yield. The ^{1}H NMR spectrum of **6** showed no signals originating from the porphyrin core, and the UV–vis. spectrum of **6** showed no detectable absorbance at 420 nm, the Soret band of the porphyrin. Elemental analysis of the hydrolysis product was consistent with a